Chiang Mai J. Sci. 2015; 42(3) : 752-760
http://epg.science.cmu.ac.th/ejournal/
Contributed Paper

Synthesis and Characterization of Indium Oxide Nanoparticles Using Indium Nitrate and Polyvinylpyrrolidone (PVP) as Precursors

Somchai Sonsupap [a] Ekaphan Swatsitang [b,c]Santi Maensiri [d] and Kwanruthai Wongsaprom*[a]

[a] Department of Physics, Faculty of Science, Mahasarakham University, Mahasarakham, 44150, Thailand

[b] Department of Physics, Faculty of Science, Khon Kaen University, Khon Kaen, 40002, Thailand

[c] ntegrated Nanotechnology Research Center, Department of Physics, Faculty of Science, Khon Kaen University, Khon Kaen, 40002, Thailand

[d] School of Physics, Institute of Science, Suranaree University of Technology, Nakhon Ratchasima, 30000, Thailand

*Author for correspondence; e-mail: wkwanruthai@gmail.com

Received: 15 August 2013
Accepted: 29 January 2014

ABSTRACT

This paper reports the synthesis and characterization of In_2O_3 nanoparticles by a simple polymerized complex method using indium (III) nitrate and polyvinylpyrrolidone (PVP) as the starting chemicals. The precursors were calcined at different temperatures to obtain In_2O_3 nanoparticles. The XRD and electron diffraction analysis results indicated that the In_2O_3 samples had a cubic structure without any impurity phases.The FT-IR analysis result confirmed the formation of In_2O_3. TEM revealed that the In_2O_3 samples consist of crystalline particle of 15-25 nm which are weakly agglomerated. UV-vis spectroscopy was also performed to study the optical properties of synthesized In_2O_3 samples. The estimated band gap of the samples was 3.70-3.93 eV.

Keywords: indium oxide, nanoparticles, polyvinylpyrrolidone (PVP), cubic structure and transmission electron microscopy

1. INTRODUCTION

Indium oxide (In_2O_3) is a wide band gap n-type semiconductor with a direct band gap of 3.75 eV. In_2O_3 is an insulator in a stoichiometric state, but behaves as a high conductive semiconductor in its non-stoichiometric state. In_2O_3 has a cubic bixebyte structure with lattice parameter of 10.117 Å [1-2]. Apart from this, In_2O_3 in its nanostructure form exhibits noteworthy applications and is currently gaining much attention. The reason lies in the fact that nanomaterials have to exhibit many specific features in order to meet all the expectations that are related to their tiny size. Because physical and chemical properties of nanomaterials depend not only on the composition but also on the particle size and shape, a good synthesis protocol first of all needs to provide control over particle size and shape [3]. Seetha et al. [4] reported visible light emitting In_2O_3 nanoparticles synthesized

by the precipitation method. Sharma et al. [5] reported that thin films of In_2O_3 are deposited onto indium–tin oxide (ITO) coated glass substrates by the electrodeposition technique to enhance their optical properties. Huang et al. [6] prepared through the liquid precipitation method, an application for gas-sensing. Qin et al. [7] reported the fabrication and characterization of efficient organic solar cells (OSCs) based on p-type In_2O_3 films as the hole-transporting layer (HTL) by the radio frequency (RF) magnetron sputtering method.

There are a variety of synthesis techniques (routes) for preparation of In_2O_3 nanoparticles such as sol–gel [8, 9], chemical vapor deposition [10-11], hydrothermal [12-13] and electrospinning [14-16]. Recent studies on un-doped and doped In_2O_3 have mainly concentrated on preparation of various nano-structural shapes and their properties. For practical applications, a significant interest has been shown in the field of zero-dimensional and one-dimensional semiconducting In_2O_3 and indium tin oxide (ITO), such as nanospheres [5, 17], nanorods [8, 10], nanopyramids [18], nanofibers [14-16], nanowires [19] and nanoparticles [11, 19-21]. Among other established synthesis methods, simple and cost effective routes to synthesize nanocrystalline In_2O_3 by utilization of cheap, nontoxic and environmentally benign precursors are still the key issues, as well as the ability to control particle size and shape. A simple method has been successfully used by our group to synthesize CeO_2 nanoparticles with particle sizes of ~5-10 nm [22], nanocrystalline Zn and Co-doped ZnO powders with particle sizes of ~50-100 nm and nanorods with dimeters of ~100-200 nm [23-24].

In this paper, we investigated the applicability of polyvinyl pyrrolidone (PVP) in preparing In_2O_3 nanoparticles using Indium (III) nitrate n-hydrate and PVP as the starting chemicals. The synthesized precursors were calcined at 450, 500, 550 and 600°C for 2h to obtain the In_2O_3 nanoparticles. The synthesized powders were characterized by X-ray diffraction (XRD), transmission electron microscopy (TEM), ultraviolet-visible spectroscopy (UV-Vis) and fourier infrared spectroscopy (FT-IR).

2. MATERIALS AND METHODS

In this study, indium (III) nitrate n-hydrate (Kanto, 99.9%) and PVP (M_n=1300000, Aldrich) were used as the starting chemicals. In a typical procedure, 7.5 g of polyvinyl pyrrolidone (PVP) was first dissolved 500 ml distilled water under vigorous stirring at 50°C. Subsequently, 5 g of indium nitrate n-hydrate was slowly added to this solution. The transparent white-colored mixture was then stirred for several hours in air until dry. At this step, the PVP acted as a matrix for entrapment of indium ion and it generated a gelled precursor [22-24]. Throughout the whole process described above, no ph adjustment was made.

Then, the precursor was mixed well and a yellow powder can be obtained after 30 min of milling done in a mortar and pestle, by hand at room temperature. Finally, the dried precursor was calcined in a box furnace at 450, 500, 550 and 600°C for 2h in air. The calcined samples were ground to break up large agglomerates. The final products obtained were yellow white In_2O_3 nanoparticles.

In order to determine the temperature of passible decomposition and crystallization of the powders, the dried powder precursor was subjected to TG-DTA (SSDT Q600, Luken's drive, Newcastle) at a heating rate of 10°C / min in air up to 1000°C. The prepared In_2O_3 sample was characterized by X-ray diffraction at room temperature using a Philips X-ray diffractometer (PW3710, The Natherlands), working with CuKα radiation in the 2q range of 20°-90°. Fourier transform infrared (FT-IR) spectra of the powders (as pellets in KBr) were recorded using a fourier transform infrared spectrometer (PerkinElmer Instrument, England)

in the range of 4000-400 $cm^{-1}$with a resolution of 1 cm^{-1}. The particle size and morphology of the calcined powders were characterized by transmission electron microscopy (JEOL 2010, 200 kV, England). The optical absorption spectra were measured in the range of 200-800 nm using a UV-vis Spectrometer (T80/T80t, PG Instruments Limited, UK).

3. RESULTS AND DISCUSSION

The TG and DTA curves of the powder precursor of In_2O_3 are shown in Figure 1. The TG curve in Figure 1 shows a major weight loss step from ~200°C up to about ~500°C with slight weight loss from ~50°C to ~195°C, and no further weight loss was observed above 500°C. The weight loss is related to the combustion of the organic matrix. Weight loss occurs gradually at temperatures above room temperature and reaches ~15% around 200°C in Figure 1. This weight reduction is due to the loss of absorbed water (mainly from hydration of the indium nitrate used as the starting material) [13] and thermal decomposition of the surfactant polymer. The significant weight loss of ~70% in Figure 1 between ~200 to ~500°C was attributed to the complete decomposition of $In(NO_3)_3$ and the degradation of PVP, which involves both intra- and intermolecular transfer reactions. The

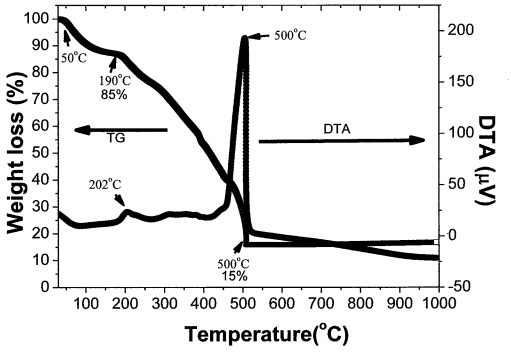

Figure 1. TG-DTA curves of the thermal decomposition of the precursor at a heating rate of 10°C/min in static air.

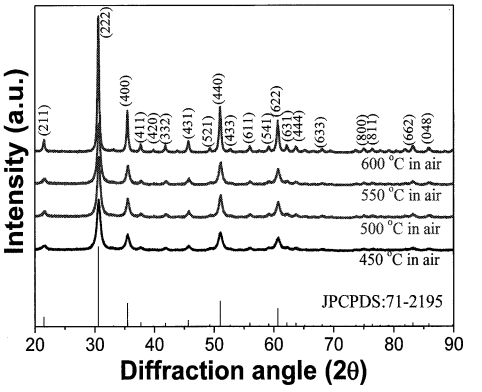

Figure 2. XRD patterns of In_2O_3 nanoparticles calcined in air for 2 h at 450°C, 500°C, 550 °C and 600°C.

exothermic peaks at 500°C in Figure 1 were the result of the oxidation of carbon and carbon monoxide released by the decomposition of PVP [16]. The structure of the In_2O_3 sample was primary examined by XRD. The XRD patterns from the In_2O_3 samples are shown in Figure 2. All of the detectable peaks (Figure 2) can be indexed as the In_2O_3 cubic structure in the standard data (JCPDS:71-2195). The cubic lattice parameters *a*, calculated from the XRD spectra are 1.0099, 1.0092, 1.0122 and 1.0119 nm for In_2O_3 samples calcined at 450, 500, 550 and 600°C, respectively. These values are close to those of lattice constant a = 1.0117 nm in the standard data (JCPDS: 71-2195). The crystallite sizes (D) of the powders were estimated from X-ray line broadening using Scherrer's equation [25].

$$D = \frac{0.89\lambda}{\beta \cos\theta} \quad (1)$$

where λ is the wavelength of the X-ray radiation, K is a constant taken as 0.89, θ is the diffraction angle, β is the full width at half maximum (FWHM), and were determined to be 12.1, 13.7, 17.1 and 23.7 nm for In_2O_3 samples calcined at 450, 500, 550 and 600°C, respectively. The crystallite sizes and lattice parameters of In_2O_3 samples are summarized in Table 1.

Table 1. Summary of particle sizes from XRD and TEM, cubic lattice constant and the band gap (E_g) of the nanocrystalline In_2O_3 samples calcined in air at different temperatures for 2h.

In_2O_3 sample	particle size (nm)		Cubic lattice parametera	Estimated band gap
	from XRD	from TEM	a(nm)	(eV)
Calcined at 450°C	12.1	15	1.0099	3.93
Calcined at 500°C	13.7	17	1.0092	3.90
Calcined at 550°C	17.1	19	1.0122	3.70
Calcined at 600°C	23.7	25	1.0119	3.82

The formation of an In_2O_3 bond was supported by FT-IR spectra as shown in Figure 3. In the FT-IR spectra absorption peaks ascribing to In-O bonds appear at wave numbers of ~475, ~564, and ~645 cm^{-1}, suggesting that the phase transformation of $In(OH)_3$-to-In-O occurs here, while C=O and N–H bonds with the PVP polymers are at ~1635 cm^{-1} and ~1109 cm^{-1} respectively [13]. These reveal that the PVP molecules adsorbed preferentially on the surface of $In(OH)_3$ crystallites. Disappearance of N–H and C-O bond from the PVP polymer at 500-600°C in Figure 3 indicates a complete removal of the polymer [22].

The morphology and structure of the In_2O_3 samples were investigated by TEM. It is clear from the TEM bright-field images (Figure 4) that the morphology and size of In_2O_3 nanoparticles were affected by the calcination temperature. The TEM bright-field images of In_2O_3 show that the In_2O_3 sample calcined at 450°C (Figure 4(a)) has nanoparticles with the smallest particle size of ~15 nm whereas at 500°C (Figure 4(c)) trains nanoparticles have sizes of ~17 nm. The In_2O_3 sample calcined at 550°C (Figure 4(e)) consists of well dispersed particles of ~19 nm and the sample calcined at 600°C (Figure 4(g)) consists of particles of ~25 nm in diameter. The corresponding selected-area electron diffraction (SAED) patterns (Figure 4 (b), (d), (f) and (h)) of all the In_2O_3 samples show spotty ring patterns without any additional diffraction spots and rings of second phases revealing their crystalline cubic structure which is in agreement with the XRD result and standard data (JCPDS:71-2195). Increase in calcination temperature results in stronger spotty patterns and the In_2O_3 samples calcined at 550 and 600°C show strong spotty patterns, indicating large particle size of highly crystalline cubic structure. The measured interplanar spacings (d_{hkl}) from selected-area electron diffraction patterns in Figure 4 are in good agreement with the values from the standard data (JCPDS:71-2195) as summarized in Table 2.

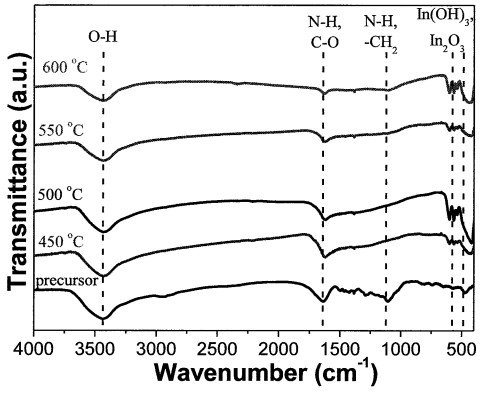

Figure 3. FTIR spectra of the In_2O_3 nanoparticles calcined at different temperatures for 2 h.

The high-resolution TEM (HRTEM) image shown in Figure 5 indicates the presence of a lattice fringe in nanoparticles of In_2O_3 sample calcined at 550°C. Lattice distances of 0.5021, 0.3483 and 0.2763 nm indicated in

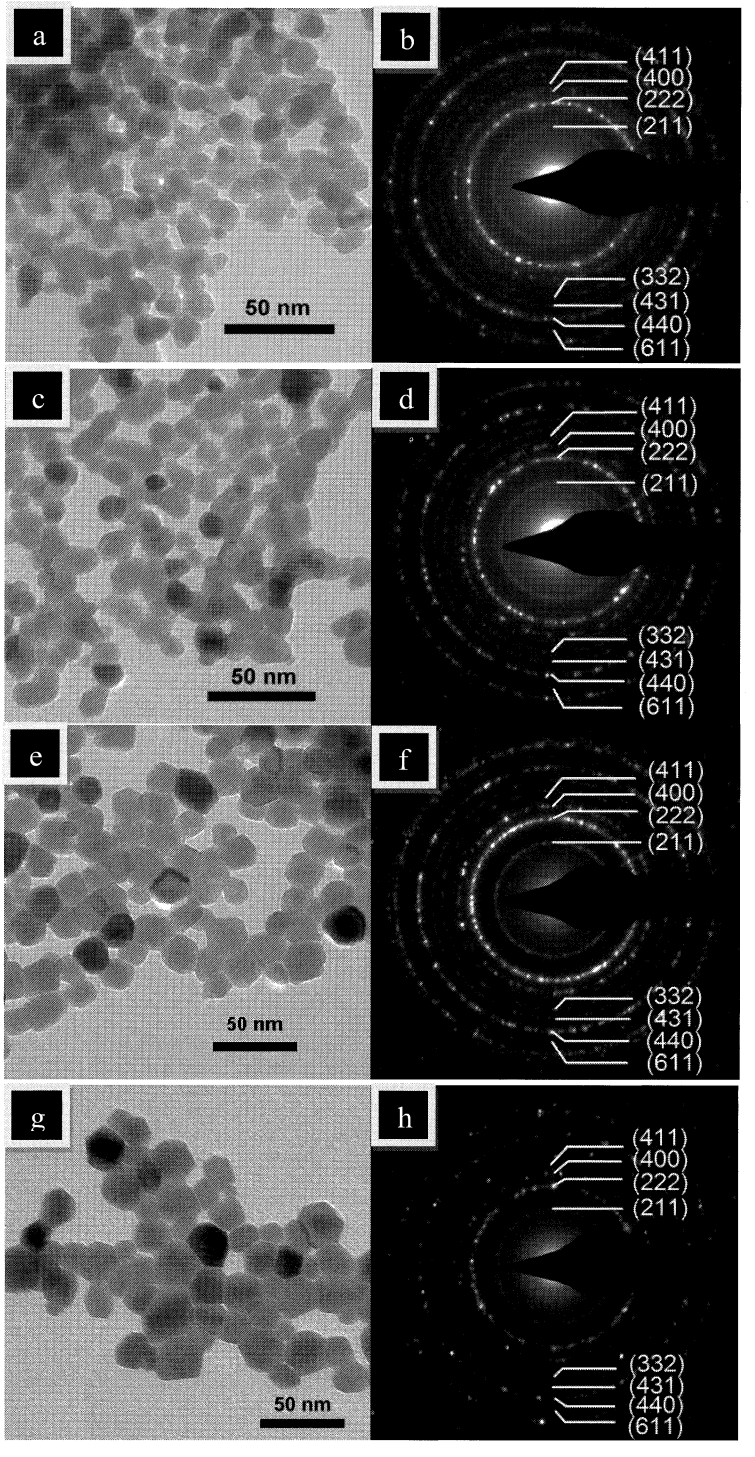

Figure 4. TEM images of In_2O_3 nanoparticles calcined at (a) 450°C, (c) 500°C, (e) 550°C, (g) 600°C, and bcc-structured polycrystalline SAED pattern of In_2O_3 nanoparticles calcined at (b) 450°C, (d) 500°C, (f) 550°C and (h) 600°C.

Table 2. Interplanar spacings (d_{hkl}) of In_2O_3 samples calculated from TEM selected-area electron diffraction patterns in Figure 4 compared with the reference values in the standard data (JCPDS:71-2195).

Ring	Calculated interplanar spacing (d_{hkl}) In_2O_3 sample (Å)				Standard data (JCPDS:71-2195)	
	Calcined at 450°C	Calcined at 500°C	Calcined at 550°C	Calcined at 600°C	d_{hkl}(Å)	hkl
1	4.006	4.059	3.944	4.070	4.130	211
2	2.837	2.864	2.863	2.857	2.920	222
3	2.471	2.491	2.483	2.481	2.529	400
4	2.330	2.334	2.326	2.344	2.384	411
5	2.117	2.139	2.107	2.113	2.157	332
6	1.930	1.949	1.939	1.943	1.984	431
7	1.748	1.766	1.759	1.755	1.788	440
8	1.604	1.616	1.610	1.619	1.641	611

these figures correspond to the (200) (220) and (321) crystalline planes of In_2O_3, respectively. These are in agreement with the standard data (JCPDS: 71-2195).

Optical properties of In_2O_3 nanoparticles were characterized using a UV–Vis spectrophotometer. In_2O_3 (Figure 6) shows a strong absorption below 350 nm (3.54 eV) with a well-defined absorbance peak at around 285 nm (4.35 eV). The band gap can be determined by fitting the absorption data to the direct transition equation by extrapolation of the linear portions of the curves so the absorption equals zero (the inset of Figure 6):

$$\alpha h\nu = A(h\nu - E_g)^{1/2} \qquad (2)$$

Where a is the optical absorption coefficient, $h\nu$ is the photon energy, E_g is the direct band gap, and E_D is a constant [26]. An extrapolation of the linear region of a plot of $(\alpha h\nu)^2$ on the Y-axis versus photon energy ($h\nu$) on the X-axis gives the value of the optical band gap (E_g). The plots of $(\alpha h\nu)^2$ and $h\nu$ are shown in Figure 6

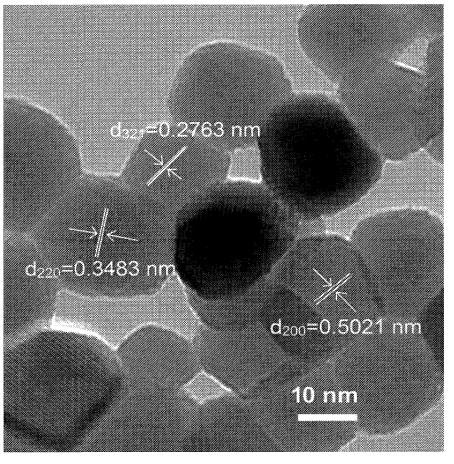

Figure 5. HRTEM image of In_2O_3 nanopaticles calcined at 550°C.

for In_2O_3 nanoparticles. The calculated values of the optical band gaps for In_2O_3 nanoparticles are ~3.93 eV, ~3.90 eV, ~3.70 eV and ~3.82 eV for the In_2O_3 samples calcined at 450, 500, 550 and 600°C, respectively. This value is higher than the bulk In_2O_3 value of 3.75 eV.

The increase in the optical band gap with increasing temperature may be due to the increase

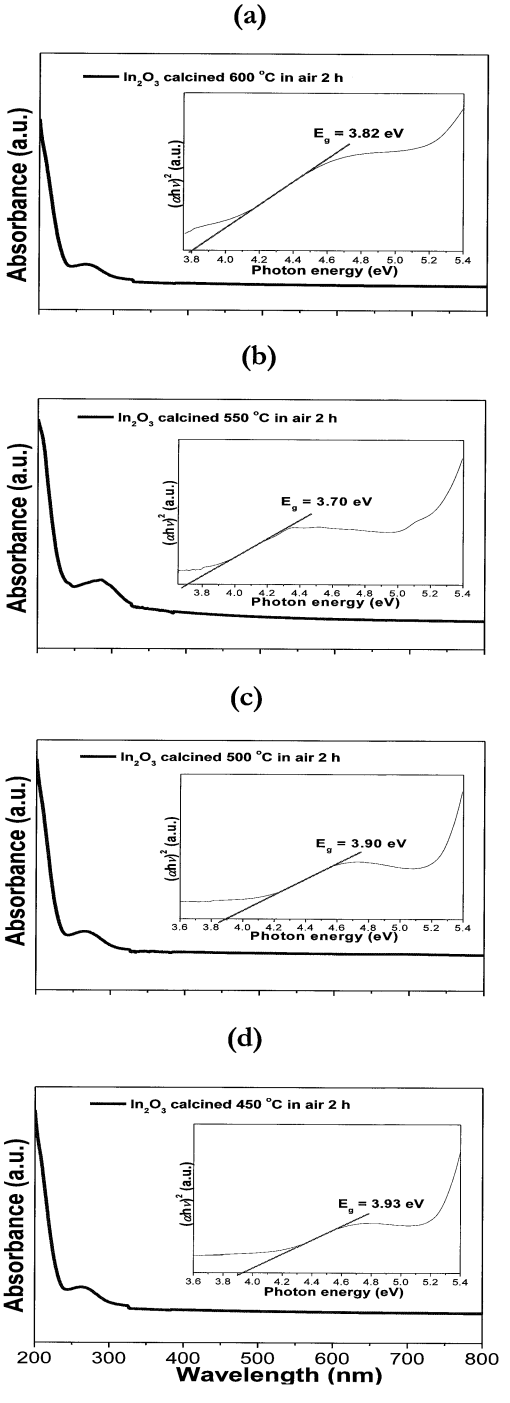

Figure 6. Room temperature optical absorbance spectra of In_2O_3 samples calcined in air for 2 h at (a) 450°C, (b) 500°C, (c) 550°C and (d) 600°C. The insets show plots of $(\alpha h\nu)^2$ as a function of photon energy.

in grain size, the reduction in the disorder and decrease in density of defect states [27-28]. The increase in the optical band gap could also be discussed on the basis of density of state model proposed by Mott and Davis [29]. The quantum size effects have been observed in In_2O_3 systems reported in the literature. For example, Maensiri et al. [30] reported band gaps of 30 and 10 nm for In_2O_3 nanoparticles prepared using reverse micelles to be 3.29 and 3.31 eV, respectively. Bagheri-Mohagheghi et al. [31] reported band gaps of 10 and 45 nm for In_2O_3 nanoparticles synthesized by the sol–gel method to be 4.32 and 4.34 eV, respectively. Since the size of the particles decreases, and the atomic wave functions are overlapping more, we may attribute this to approaching the quantum confinement limit of nano-particles. The quantum confinement effect is expected for semiconducting nanoparticles, and the absorption edge will be shifted to a shorter wavelength (higher energy) when the particle size decreases.

4. CONCLUSION

We have synthesized nanoparticles of In_2O_3 by a simple method using indium (III) nitrate and polyvinyl polyhedron (PVP) as the starting chemicals. Structural, morphological and optical properties of the synthesized nanoparticles were characterized. XRD and TEM analysis showed that the In_2O_3 samples exhibited a single phase polycrystalline nature with particle sizes of 12 – 25 nm. The morphology and size of In_2O_3 materials were affected by the calcination temperature. The optical band gap of synthesized powders exhibited a direct band gap (E_g) which was determined to be 3.70-3.93 eV.

ACKNOWLEDGMENT

The authors would like to thank the Department of Chemistry, Mahasarakham University for providing TG-DTA and UV-

vis facilities, Department of Physics, Khon Kaen University for providing TEM facilities. This work was supported by Mahasarakham University Thailand.

REFERENCES

[1] Hamburg I. and Granqvist C. G., Evaporated Sn-doped In_2O_3 films: Basic optical properties and applications to energy-efficient windows, *J. Appl. Phys.,* 1986; **60**: R123-R160. DOI 10.1063/1.337534.

[2] Young S. C. and Young D. H., Controlled-synthesis and photocatalytic properties of h-In_2O_3 and c-In_2O_3, *Bull. Kor. Chem. Soc.,* 2010; **3**: 1769-1172. DOI 10.5012/bkcs.2010.31.6.1769.

[3] Niederberger M., Garnweitner G., Buha J., Polleux J., Ba J. and Pinna N., Nonaqueous synthesis of metal oxide nanoparticles:Review and indium oxide as case study for the dependence of particle morphology on precursors and solvents, *J. Sol-Gel Sci. Technol.,* 2006; **40**: 259-266. DOI 10.1007/s10971-006-6668-8.

[4] Seetha M., Bharathi S., Raj A. D., Mangalaraj D., Nataraj D., Optical investigations on indium oxide nano-particles prepared through precipitation method, *Mater. Charact.,* 2009; **60**: 1578–1582. DOI 10.1016/j.matchar.2009.09.009.

[5] Sharma R., Mane R. S., Sun K. M., Sung H. H., Optimization of growth of In_2O_3 nano-spheres thin films by electrodeposition for dye-sensitized solar cells, *J. Alloys Compd.,* 2009; **479**: 840-843. DOI 10.1016/j.jallcom.2009.01.070.

[6] Huang S. Z., Lin W. and Chen W. Z., Gas sensitivity of indium oxide, *Trans. Nonferrous Met. Soc. China,* 2009; **19**: s80-s82. DOI 10.1016/S1003-6326(10)60249-X.

[7] Qin P., Fang G., Sun N., Fan X., Zheng Q., Cheng F., Wan J. and Zhao X., P-type indium oxide thin film for the hole-transporting layer of organic solar cells, *Thin Solid Films*, 2012; **520**: 3118-3124. DOI 10.1016/j.tsf.2011.12.044.

[8] Cheng Z. X., Xiang B. D., Qing Y. P., Jian C. Z. and Xiao W. D., Preparation and characterization of In_2O_3 nanorods, *Mater. Lett.,* 2006; **60**: 3137-3140. DOI 10.1016/j.matlet.2006.02.065.

[9] Niu X., Zhong H., Wang X. and Jiang K., Sensing properties of rare earth oxide doped In_2O_3 by a sol–gel method, *Sens. Actuators, B.*, 2006; **15**: 434-438. DOI 10.1016/j.snb.2005.10.004.

[10] Jae M. K., Joung K. P., K. N. K., Chang H. K. and Ho G. J., Synthesis of In_2O_3 nano-materials with various shapes, *Curr. Appl. Phys.,* 2006; **6S1**: e198–e201. DOI 10.1016/j.cap.2006.01.039.

[11] Wang Ch.Y., Ali M., Kups Th., Röhlig C.-C., Cimalla V., Stauden Th. and Ambacher O., NO_x sensing properties of In_2O_3 nanoparticles prepared by metal organic chemical vapor deposition, *Sens. Actuators, B.,* 2008; **130**: 589-593. DOI 10.1016/j.snb.2007.10.015.

[12] Sorescu M., Diamandescu L. and Tarabasanu-Mihaila D., α-Fe_2O_3–In_2O_3 mixed oxide nanoparticles synthesized under hydrothermal supercritical conditions, *J. Phys. Chem. Solids.*, 2004; **65**: 1719-1725. DOI 10.1016/j.jpcs.2004.05.002.

[13] Tseng T.-T. and Tseng W. J., Effect of polyvinylpyrrolidone on morphology and structure of In_2O_3 nanorods by hydrothermal synthesis, *Ceram. Int.,* 2009; **35**: 2837-2844. DOI 10.1016/j.jpcs.2004.05.002.

[14] Zhang Y., Li J., Li Q., Zhu L., Liu X., Zhong X., Menga J. and Cao X., Preparation of In_2O_3 ceramic nanofibers by electrospinning and their optical properties, *Scripta Mater.,* 2007; **56**: 409-412. DOI 10.1016/j.scriptamat.2006.10.032.

[15] Xu L., Dong B., Wang Y., Bai X., Liu Q. and Song H., Electrospinning preparation and room temperature gas sensing properties of porous In_2O_3 nanotubes and nanowires, *Sensor Actuat. B: Chem.*, 2010; **147**: 531-538. DOI 10.1016/j.snb.2010.04.003.

[16] Li Z., Fan Y. and Zhan J., In_2O_3 Nanofibers and Nanoribbons: Preparation by electrospinning and their formaldehyde gas-sensing properties, *Eur. J. Inorg. Chem.,* 2010; **2010**: 3348-3353. DOI 10.1016/j.snb.2012.03.055.

[17] Souza E.C.C., Rey J.F.Q. and Muccillo E.N.S., Synthesis and characterization of spherical and narrow size distribution indium oxide nanoparticles, *Appl. Surf. Sci.,* 2009; **255**: 3779-3783. DOI 10.1016/j.apsusc.2008.10.039.

[18] Qurashia A., El-Maghrabyb E.M., Yamazakia T and Kikutaa T., Catalyst-free shape controlled

synthesis of In_2O_3 pyramids and octahedron: Structural properties and growth mechanism, *J. Alloys Compd.,* 2009; **480**: L9-L12. DOI 10.1016/j.jallcom.2009.01.112.

[19] Zhanga Y., Agoa H., Liub J., Yumura M., Uchida K., Ohshima S., Iijima S., Zhu J. and Zhang X., The synthesis of In, In_2O_3 nanowires and In_2O_3 nanoparticles with shape-controlled, *J. Cryst. Growth,* 2004; **264**: 363-368.DOI 10.1016/j.jcrysgro.2004.01.025.

[20] Chandradass J., Bae D. S. and Kim K. H., A simple method to prepare indium oxide nanoparticles: Structural, microstructural and magnetic properties, *Adv. Powder Technol.,* 2011; **22**: 370-374. DOI 10.1016/j.apt.2010.05.006.

[21] Yu B., Zhu C., Gan F. and Huang Y., Optical limiting properties of In_2O_3 nanoparticles under cw laser, *Opt. Mater.,* 1997; **7**: 103-107. DOI 10.1016/S0925-3467(96)00067-5.

[22] Phoka S., Laokul P., Swatsitang E., Promarak V., Seraphin S., Maensiri S., Synthesis, structural and optical properties of CeO_2 nanoparticles synthesized by a simple polyvinyl pyrrolidone (PVP) solution route, *Mater. Chem. Phys.,* 2009; **115**: 423-428. DOI 10.1186/1556-276X-7-425.

[23] Maensiri S., Laokul P., Promarak V., Synthesis and optical properties of nanocrystalline ZnO powders by a simple method using zinc acetate dihydrate and poly (vinyl pyrrolidone), *J. Cryst. Growth*, 2006; **289**: 102-106. DOI 10.1016/j.jcrysgro.2005.10.145.

[24] Maensiri S., Laokul P., Phoka S., A simple synthesis and magnetic behavior of nanocrystalline $Zn_{0.9}Co_{0.1}O$ powders by using Zn and Co acetates and polyvinyl pyrrolidone as precursors, *J. Magn. Magn. Mater.*, 2006; **305**: 381-387. DOI 10.1016/j.jmmm.2006.01.115.

[25] Cullity B. D. and Stock R., *Elements of X-ray Diffraction*, 3rd Edn., Printice Hall: New Jersey, 2001, p. 388.

[26] Ziegler E., Heinrich A., Oppermann H. and Stover G., Electrical properties and non-stoichiometry in ZnO single crystals, *Phys. Status Solidi A.*, 1981; **66**: 635-648. DOI 10.1002/pssa.2210660228.

[27] Ilyas M., Zulfequar M., Husain M., Optical investigation of a-Ga_xSe_{100-x} thin films, *J. Mod. Opt.*, 2000; **47**: 663-675. DOI 10.1080/09500340008233387.

[28] Nang T.T., Okuda M., Matsushita T. and Suzuki A., Electrical and optical properties of Ge_xSe_{1-x} amorphous thin films, *Jpn. J. Appl. Phys.* 1976; **15:** 849-853. DOI 10.1143/JJAP.15.849.

[29] Mott N. F. and Davis E. A., *Electronics Processes in Non- Crystalline Materials,* Oxford:Clarendon, 1979.

[30] Maensiri S., Laokul P., Klinkaewnarong J., Phokha S., Promarak V. and Seraphin S., Indium oxide (In_2O_3) nanoparticles using *Aloe vera* plant extract: Synthesis and optical properties, *J. Optoelectron. Adv. M.,* 2008; **10**: 161–165.

[31] Bagheri-Mohagheghi M.-M., Shahtahmasebi N., Mozafari E.and Shokooh-Saremi M., Effect of the synthesis route on the structural properties and shape of the indium oxide (In_2O_3) nanoparticles, *Physica E.,* 2009; **41**: 1757-1762. DOI 10.1016/j.physe.2009.06.009.